14

BNWL-1010
UC-23

PACIFIC NORTHWEST LABORATORY DIVISION OF ISOTOPE DEVELOPMENT PROGRAMS QUARTERLY REPORT: NOVEMBER 1968 – JANUARY 1969

FEBRUARY 1969

AEC RESEARCH & DEVELOPMENT REPORT

BATTELLE NORTHWEST
BATTELLE MEMORIAL INSTITUTE PACIFIC NORTHWEST LABORATORY
BATTELLE BOULEVARD, P.O. BOX 999, RICHLAND, WASHINGTON 99352

BNWL-1010

LEGAL NOTICE

This report was prepared as an account of Government sponsored work. Neither the United States, nor the Commission, nor any person acting on behalf of the Commission:

A. Makes any warranty or representation, expressed or implied, with respect to the accuracy, completeness, or usefulness of the information contained in this report, or that the use of any information, apparatus, method, or process disclosed in this report may not infringe privately owned rights; or

B. Assumes any liabilities with respect to the use of, or for damages resulting from the use of any information, apparatus, method, or process disclosed in this report.

As used in the above, "person acting on behalf of the Commission" includes any employee or contractor of the Commission, or employee of such contractor, to the extent that such employee or contractor of the Commission, or employee of such contractor prepares, disseminates, or provides access to, any information pursuant to his employment or contract with the Commission, or his employment with such contractor.

PACIFIC NORTHWEST LABORATORY
RICHLAND, WASHINGTON
operated by
BATTELLE MEMORIAL INSTITUTE
for the
UNITED STATES ATOMIC ENERGY COMMISSION UNDER CONTRACT AT(45-1)-1830

ACE-R, RICHLAND, WASH.

3 3679 00061 2715

BNWL-1010

UC-23, Radioisotope and
Radiation Applications

PACIFIC NORTHWEST LABORATORY
DIVISION OF ISOTOPE DEVELOPMENT PROGRAMS
QUARTERLY REPORT: NOVEMBER 1968-JANUARY 1969

Edited by K. Drumheller

APR 2 '69

February 1969

BATTELLE MEMORIAL INSTITUTE
PACIFIC NORTHWEST LABORATORY
RICHLAND, WASHINGTON 99352

Printed in the United States of America
Available from
Clearinghouse for Federal Scientific and Technical Information
National Bureau of Standards, U.S. Department of Commerce
Springfield, Virginia 22151
Price: Printed Copy $3.00; Microfiche $0.65

ABSTRACT

PROMETHIUM OXIDE PROPERTIES

Phase Studies

The high temperature differential thermal analysis apparatus for performing phase studies on the Pm_2O_3 - Sm_2O_3 system was completed and placed in operation. A series of measurements on Sm_2O_3 showed three endothermal reactions on heating, all of which were reversible on cooling and quite reproducible. During melting experiments on Pm_2O_3 in a vacuum of above 10 μ, the sample completely vaporized during a few minutes at above 2000 °C.

Property Measurements

Development of the Knudsen cell vapor pressure apparatus continued. Temperatures as high as 2160 °C were reached in the crucible while pressures in the 10^{-6} torr range were maintained.

PROMETHIUM METAL

Preparation of Promethium Metal

A formal report, "Preparation of ^{147}Pm Metal and Determination of the Density and Melting Point," by E. J Wheelwright has been issued.

Phase Studies

The structure of promethium metal at room temperature has been successfully indexed from 14 diffraction lines as double hexagonal.

Melting Point Measurements

The newly measured melting point of promethium metal (1168 °C) fills an important vacancy in the periodic chart and aids in the theoretical interpretation of the melting point behavior of the lanthanide elements.

Hardness Measurements

Hardness measurements were made on as-cast promethium metal. An average hardness value of 63 KHN was obtained.

PROMETHIUM OXIDE COMPATIBILITY

Promethium Oxide Hydrolysis

A minimum dissolution rate in water of 8 $\mu g/cm^2$-hr was determined for Pm_2O_3 powder fired at 1000 °C.

PRODUCTION TECHNOLOGY

Promethium Purification

The promethium batch size has been increased from 240,000 to 350,000 Ci per run.

NONDESTRUCTIVE TESTING

Advanced NDT Methods

Investigation of the longitudinal and shear components of acoustic emissions to improve acoustic-emission monitoring techniques was concluded. The development of a portable acoustic-emission monitoring system was initiated. A feasibility experiment was conducted to identify the problems involved in monitoring acoustic emission from a specimen at high temperature.

CIRCULATORY SUPPORT SYSTEMS

Promethium Systems

Pertinent experiments and theoretical dose-rate data for completing the final report on promethium systems were compiled.

Other Radioisotopes

A review of the literature on fission neutron dosimetry, to better define the problems expected in the ^{238}Pu dosimetry programs, was continued.

Modification of Promethium Isotopic Composition

The ^{146}Pm to ^{147}Pm ratios for three Hanford targets analyzed thus far varied from 0.14×10^{-6} to 0.19×10^{-6}. These results indicate that some ^{146}Pm burnout has occurred but not as much as expected.

PRODUCTION OF TRANSURANIUM ELEMENTS IN LIGHT WATER REACTORS

^{241}Am and ^{238}Pu Availability

The ^{241}Am and ^{238}Pu availabilities have been recalculated assuming the additional six months ^{241}Am accumulation from ^{241}Pu decay. The total annual ^{238}Pu availability from all sources is estimated to be 1876 kg/yr in 1990.

^{250}Cf and ^{252}Cf Availability

The concentrations of all of the curium, beryllium, and californium isotopes involved in the ^{252}Cf production chain have been calculated with the ALTHAEA program for both PWR and BWR equilibrium fuel cycles. The annual availability of ^{252}Cf is estimated to be 291.0 μg/yr in 1990.

NEPTUNIUM-237 PRICING

^{237}Pu Cost Calculations

The cost of producing ^{238}Pu by target irradiation of ^{237}Np in a PWR for a range of cost parameters was calculated with the TAIRCOST program.

^{236}Pu in ^{238}Pu

An evaluation of the ALTHAEA program's ability to track experimental ^{236}Pu data was carried out.

FISSION PRODUCT RHODIUM AND PALLADIUM

Radiation Characteristics of Fission Product Rh and Pd

Work has been started on the evaluation of the radiation characteristics of fission-product rhodium and palladium from power reactors.

TABLE OF CONTENTS

LIST OF FIGURES ix
LIST OF TABLES ix
INTRODUCTION xi
PROMETHIUM OXIDE PROPERTIES 1
Phase Studies 1
Property Measurements 5
PROMETHIUM METAL PROPERTIES 7
Preparation of Pm Metal 7
Phase Studies 7
Melting Point Measurements 8
Hardness Measurements 10
PROMETHIUM OXIDE COMPATIBILITY 13
Promethium Oxide Hydrolysis 13
PRODUCTION TECHNOLOGY 15
Promethium Purification 15
NONDESTRUCTIVE TESTING 17
Advanced NDT Methods 17
CIRCULATORY SUPPORT SYSTEMS 27
Promethium Systems 27
Other Radioisotopes 27
Modification of Promethium Isotopic Composition . . . 28
PRODUCTION OF TRANSURANIUM ELEMENTS IN LWR'S 29
^{241}Am and ^{238}Pu Availability 29
^{250}Cf and ^{252}Cf Availability 30
^{237}Np PRICING 33
^{238}Pu Cost Calculations 33
^{236}Pu in ^{238}Pu 34
FISSION PRODUCT RHODIUM AND PALLADIUM 39
Radiation Characteristics of Fission Product Rh and Pd 39
DISTRIBUTION 41

LIST OF FIGURES

1	Overall View of High Temperature Differential Thermal Analyses (DTA) Apparatus.	2
2	Induction Coil and Eddy Current Concentrator of DTA System	3
3	DTA Sample Block (Graphite) and Heat Shields (Tungsten). Sample Cups Inserted in Block Are Tungsten or Alumina.	4
4	Melting Points of Rare Earth Metals	9
5	Effect of Feed Dilution and Resin Cross-Linkage or Resin Capacity.	16
6	Examples of Crack Tip Location Using Longitudinal-Shear Acoustic Emission Components.	19
7	Experimental Arrangement for Receiving Acoustic Emission from a High Temperature Source.	22
8	Acoustic Emission Caused by Thermal Cycling a Weld Coupon of 316 SS (weld metal contaminated by titanium).	23
9	Surface Wave Transmission of Acoustic Coupler as a Function of Temperature.	25

LIST OF TABLES

1	Effect of Feed Dilution on Promethium Batch Size	15
2	Annual Availability of ^{241}Am and ^{238}Pu	30
3	Isotopic Concentrations in Power Reactor Fuels	31
4	Annual Availability of ^{250}Cf and ^{252}Cf, μg/yr.	32
5	Base Cost Sets for ^{238}Pu Production Cost Calculations	34
6	Variation of ^{238}Pu Production Cost with ^{237}Np Target Irradiation Cost Parameters	35
7	Comparison of ALTHAEA Calculations with Yankee Experimental Data on $^{236}Pu/^{238}Pu$ Compositions	36

PACIFIC NORTHWEST LABORATORY
DIVISION OF ISOTOPE DEVELOPMENT PROGRAMS
QUARTERLY REPORT: NOVEMBER 1968 - JANUARY 1969

Edited by K. Drumheller

INTRODUCTION

This is the ninth report of a series initiated in 1966 to provide detailed and timely information on the results of the isotopic fuels program and related research being conducted at the Pacific Northwest Laboratory by Battelle-Northwest for the U.S. Atomic Energy Commission. The previous reports of the series are BNWL-385, 466, 570, 680, 681, 781, 877, and 924.

This report covers the three-month period, November 1968 through January 1969.

PROMETHIUM OXIDE PROPERTIES

PHASE STUDIES

C. E. McNeilly

The high temperature differential thermal analysis (DTA) apparatus, patterned after that of Rupert at Los Alamos,[1] for performing phase studies on the Pm_2O_3-Sm_2O_3 system has been completed and placed in operation. An overall view of the apparatus installed in the glove box, a close-up of the current concentrator in the vacuum system with the induction coil, and the graphite sample holder and heat shields are shown in Figures 1, 2 and 3, respectively.

The sample, in the form of a powder or solid particles, is placed in a tungsten or rhenium cup in one of the cavities of the graphite holder while the other cavity is left empty. In operation, reverse biased photo-diodes look at the two cavities while an automatic optical pyrometer looks at the lid of the container. The pyrometer output is part of a closed control loop with the induction generator so that the temperature can heat, soak, or cool according to a predetermined program. The temperature difference between the sample and the graphite is obtained by subtracting the amplified output of one diode from the other. This difference is plotted on the vertical axis of a storage oscilloscope while the temperature of the graphite is marked on the horizontal axis. An endo- or exo-therm representing a phase transformation then appears as a peak on the oscilloscope trace.

Calibration of the DTA apparatus was completed by using the liquid $\rightleftarrows$ solid transition points of gold (1063 °C), platinum (1774 °C), alumina (2040 °C), and iridium (2454 °C). Reproducibility varied from about ±6 °C at the gold point up to about ±20 °C at the iridium melting point. A series of measurements on Sm_2O_3 showed three endothermal reactions on heating,

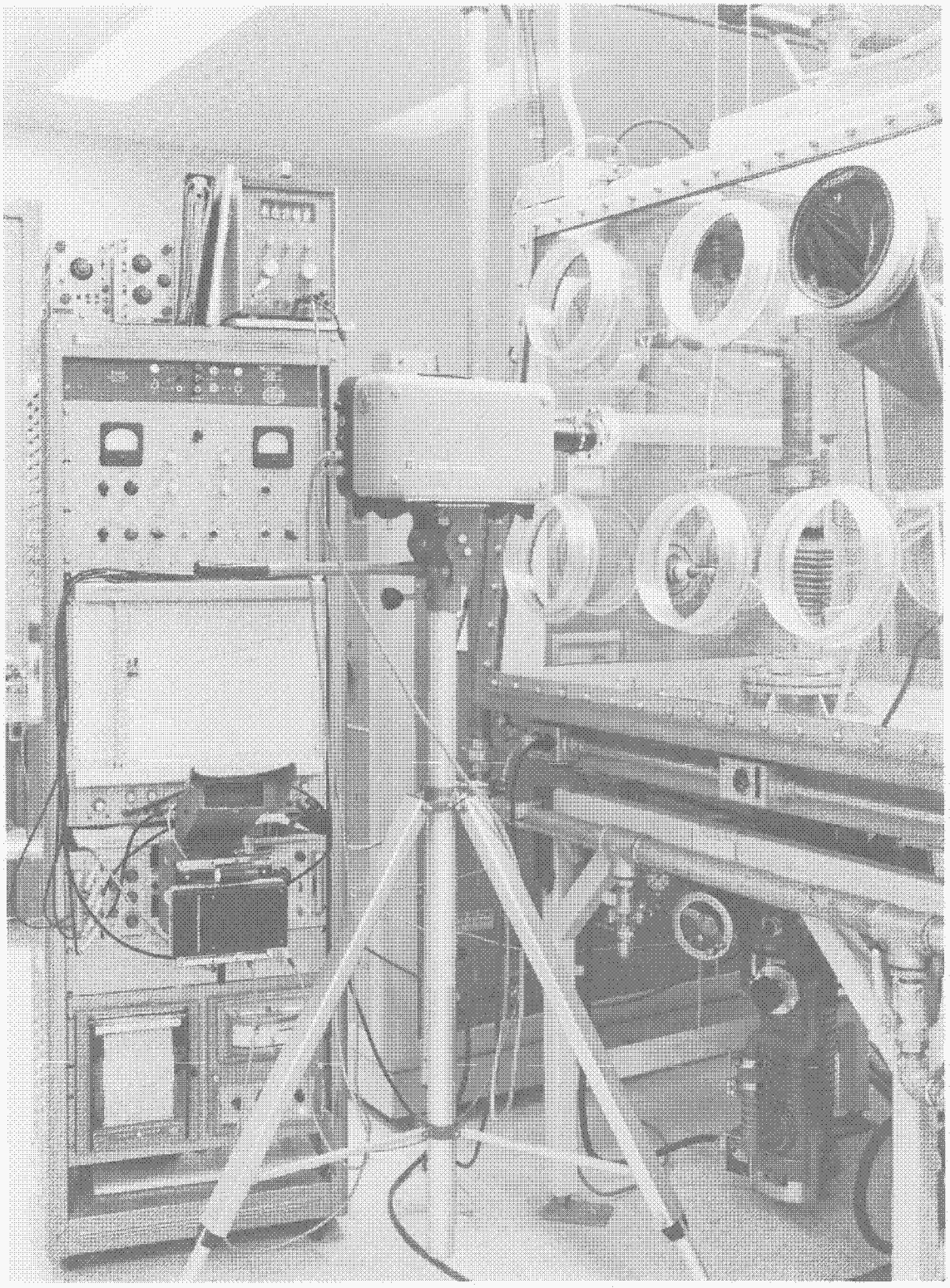

Neg 0684229-1

FIGURE 1. Overall View of High Temperature Differential Thermal Analyses (DTA) Apparatus.

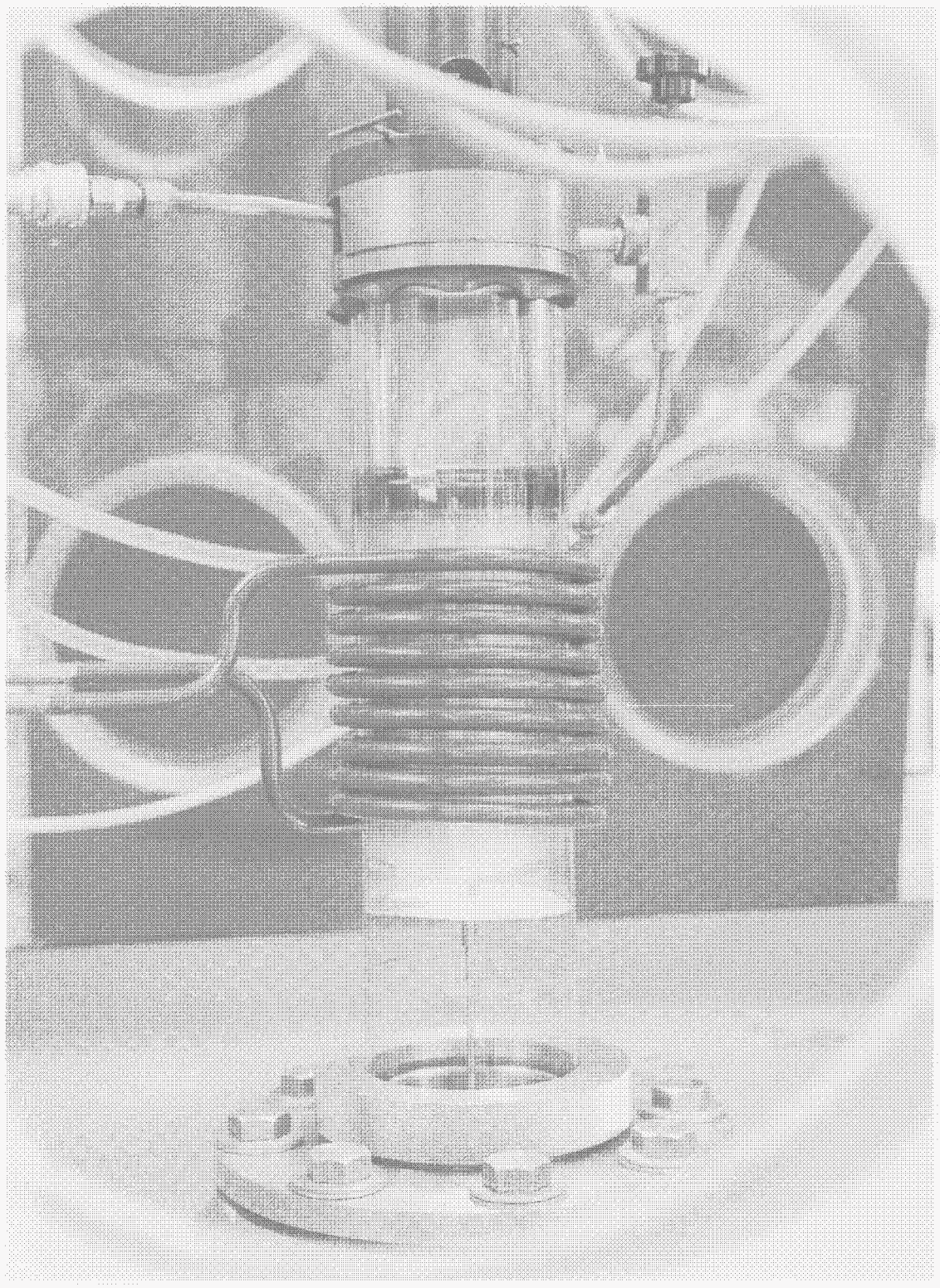

Neg 0684229-3

FIGURE 2. Induction Coil and Eddy Current Concentrator of DTA System.

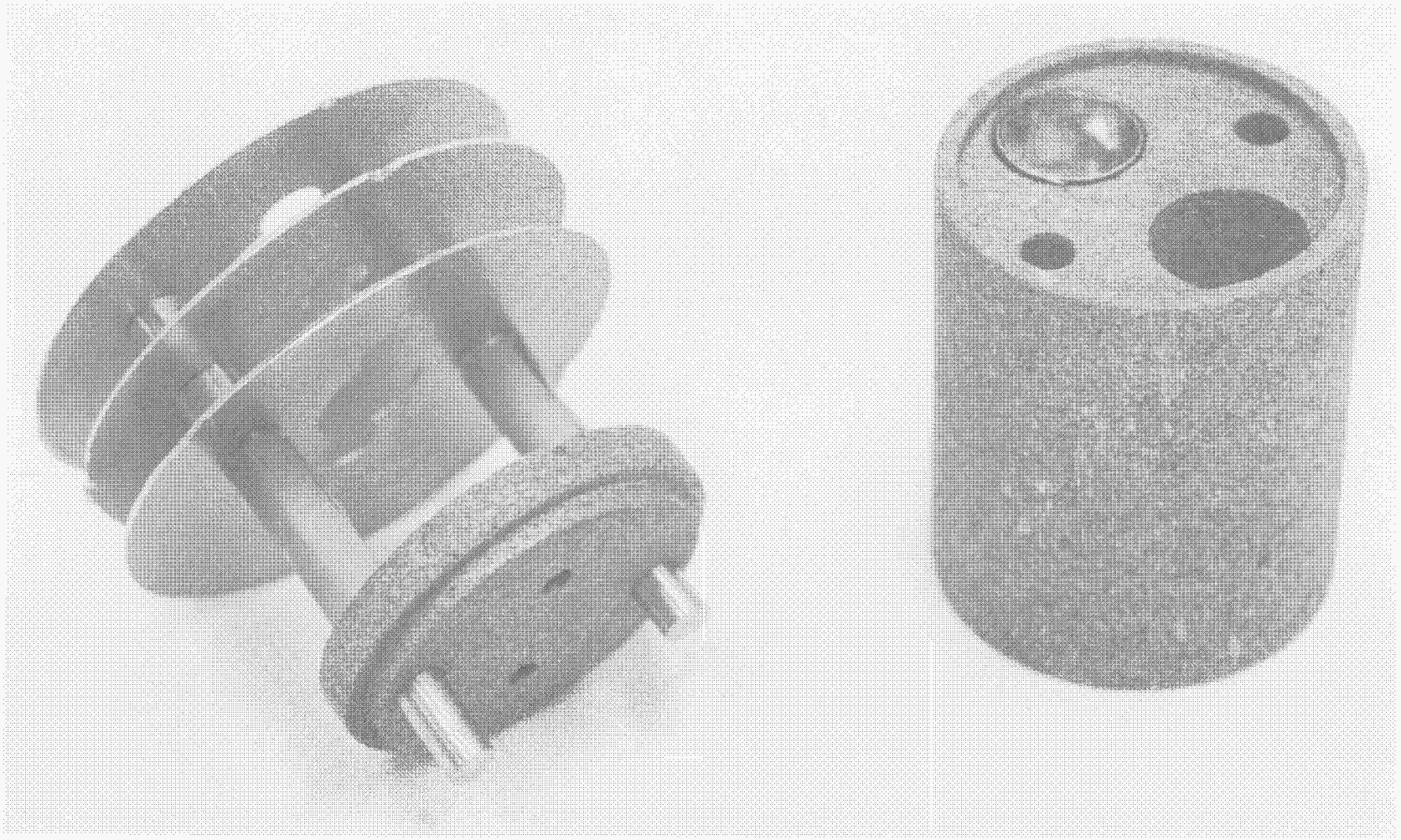

Neg 0684229-4

FIGURE 3. DTA Sample Block (Graphite) and Heat Shields (Tungsten). Sample Cups Inserted in Block Are Tungsten or Alumina.

coupling between the sensors and the DCB specimen. The couplant used for both sensors was Eastman 910 Pressure Sensitive Cement. When precautions were taken to obtain a very thin layer of couplant between the sensor and the specimen, the longitudinal components of the emissions appeared to be about twice the amplitude of the shear component of the same emissions. Figure 6 shows two representative examples comparing the longitudinal and shear components of individual acoustic-emission signals.

The ability to simultaneously receive and display separately the longitudinal and shear components of acoustic emission makes possible the location of the source of that emission if it occurs along a known line, such as the lengthwise groove in the DCB specimen used in these experiments or along a weld seam. Since the shear component of the emission signal travels slower than the longitudinal component, the time between the arrival of the longitudinal and shear components is a function of the distance between the source of the emission and the sensors receiving the signal. The following equation demonstrates this relationship:

$$D = \frac{t}{\frac{1}{V_S} - \frac{1}{V_L}}$$

where D = distance to crack tip

t = time between arrival of longitudinal and shear components

V_S = shear velocity in material

V_L = longitudinal velocity in material.

This relationship was applied to the two signal pairs shown in Figure 6A and B to obtain the results shown directly beneath each photograph. The signals shown were recorded on a dual beam oscilloscope. The signal pair in Figure 6A was recorded by triggering the oscilloscope from a third transducer mounted

NONDESTRUCTIVE TESTING

ADVANCED NDT METHODS

W. D. Jolly

Investigation of the longitudinal and shear components of acoustic emissions to improve acoustic-emission monitoring techniques was concluded. The acoustic-emission analysis system was used in these experiments to evaluate the limitations on acoustic-emission monitoring imposed by material properties, sensors, and signal processing electronics. Experiments performed with the system showed that acoustic emissions can be as short as 0.2 μsec in duration and contain frequencies as high as 30.0 MHz. Other experiments were performed with the analysis system to determine the variation of polarization of the shear component of acoustic emissions and to compare the shear component amplitude with the longitudinal component amplitude of the emission signal. The system was also used to demonstrate a method of locating and following the propagation of a fracture along a previously determined line.

The variation of polarization of the shear component of acoustic emission from a double cantilever beam specimen of A-212-B was found to be predominantly perpendicular to the specimen's surface. Two PZT-5 shear transducers polarized mutually perpendicular and mounted on the free end of the DCB specimen were used to compare the amplitude of the two polarizations for individual emission signals. Polarization of the acoustic emissions appear to vary approximately ±45°.

The predominant polarization of the shear component was compared to the longitudinal component of the same signals by using a 2 MHz PZT-5 longitudinal sensor mounted next to the shear sensors. Longitudinal signals were generally lower in amplitude than the vertically polarized shear signals. The signal amplitude from both sensors was found to depend on the

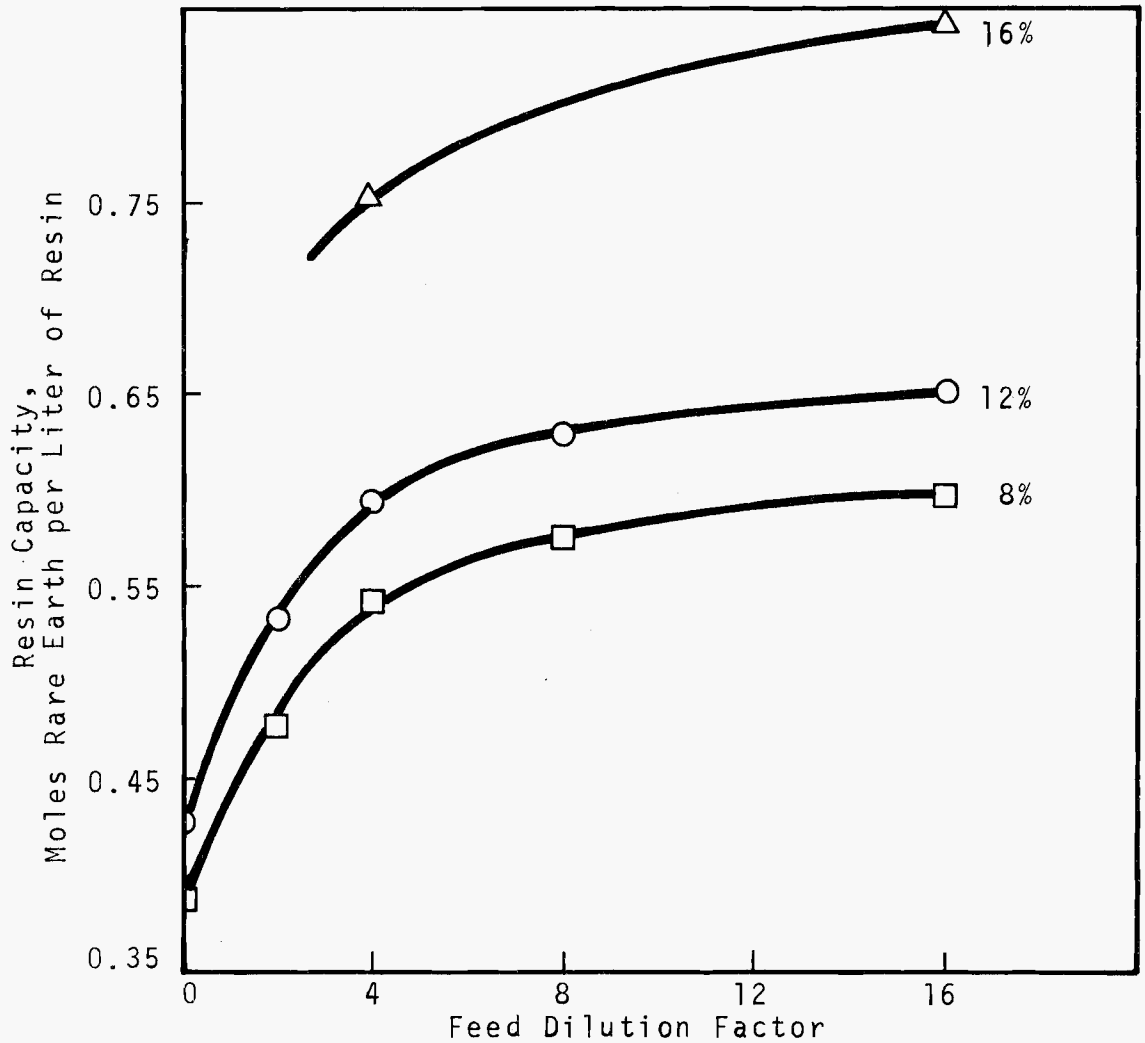

FIGURE 5. Effect of Feed Dilution and Resin Cross-Linkage on Resin Capacity.

PRODUCTION TECHNOLOGY

PROMETHIUM PURIFICATION - D. E. Deonigi

The principal effort to improve the promethium recovery and purification during this quarter was to increase the batch size. Because of the high Na^+ and H^+ content of the current crude feed, the batch size was limited to 240,000 Ci promethium per run. To complete the partial purification of all the crude promethium on hand in Fiscal Year 1969, it is essential that this be increased to at least 300,000 Ci/run.

Our investigation showed that the batch size can be increased both by dilution of the crude feed with water and by use of higher cross-linked resin in the feed absorption column. The results summarized in Figure 5 were obtained by using a synthetic feed on a laboratory scale column.

The effect of feed dilution has been tested in full scale runs in the Promethium Recovery Facility and are in good agreement with the laboratory tests. The results of the full-scale runs are shown in Table 1.

TABLE 1. Effect of Feed Dilution on Promethium Batch Size

Feed Dilution	Promethium Recovered Ci
None	240,000
1:2	285,000
1:4	358,000

Because of the limitations of the present equipment, dilutions greater than 1:4 are not possible.

Full scale tests of the effect of resin cross-linkage will take place early in the third quarter of Fiscal Year 1969.

PROMETHIUM OXIDE COMPATIBILITY

PROMETHIUM OXIDE HYDROLYSIS

H. T. Fullam and F. P. Roberts

An attempt was made to measure the dissolution rate of Pm_2O_3 powder by counting techniques. Three batches of oxide powder were prepared and calcined at 700 °C, 850 °C, and 1000 °C, respectively. X-ray diffraction shows all three batches of oxide had the monoclinic structure. The procedure used in measuring the dissolution rate begins with weighing a certain amount of Pm_2O_3 and placing it in a measured volume of distilled water (thermostated bath). The oxide slurry is stirred continuously with a magnetic stirrer, and samples are taken every half hour. They are then centrifuged to remove the solids and a sample of the supernate is taken. The concentration of dissolved promethium in the supernate is determined by counting techniques.

Unfortunately, for each batch of oxide, the promethium concentration in each time sample was the same within the experimental error of the method. This indicates that the solution had reached the solubility limit of promethium within the first half hour. From the measured promethium concentration and an assumed maximum time of 0.5 hr to reach the solubility limit, a minimum dissolution rate of approximately 8 $\mu g/cm^2$-hr can be estimated for the oxide. However, the dissolution rate could be much greater than this since the solubility limit may have been reached in less than 0.5 hr.

REFERENCES

1. C. Rupert. Rev. Sci. Instr., vol. 36, p. 1629. 1965.

2. Pacific Northwest Laboratory Division of Isotope Development Programs Quarterly Report: August - September 1968, BNWL-924. Battelle-Northwest, Richland, Washington, November 1968.

3. E. J Wheelwright. Preparation of ^{147}Pm Metal and Determination of the Density and Melting Point, BNWL-959. Battelle-Northwest, Richland, Washington, 1968.

configuration. Samarium and, to a lesser degree, lanthanum, exhibit a statistical tendency to yield to a similar shift, and they melt 223 and 65 °C lower, respectively, than they would without such a transition.

Assuming all the lanthanides were "normal," there appears to be two linear related series, cerium through europium and gadolinium through lutecium. Perhaps, as the first six unpaired 4f electrons are added, the shielding of the bonding electrons varies in a linear fashion and melting points reflect this change. At gadolinium, the final unpaired electron completes the level and initiates a new series with a different shielding pattern for the bonding electrons; however, this does not explain the behavior of lanthanum. The crystal field effects upon the bonding electrons may be more pronounced in the absence of a 4f electron (Figure 4). The measured values are shown as solid data points, with the shifts to hypothetical "normal" positions shown by the dashed lines.

HARDNESS MEASUREMENTS

T. D. Chikalla

Hardness measurements were made on as-cast promethium metal. The metal disc was cut from a cast rod and metallographically polished. A thin film of silicone oil was placed over the metal surface to prevent oxidation from the air environment in the cell containing the hardness tester. Seventeen indents were made by using a standard Knoop hardness tester with a 500 g load, and an average hardness value of 63 KHN was obtained. A similar test was made on an as-cast rod of samarium metal; it yielded a hardness of 45 KHN.

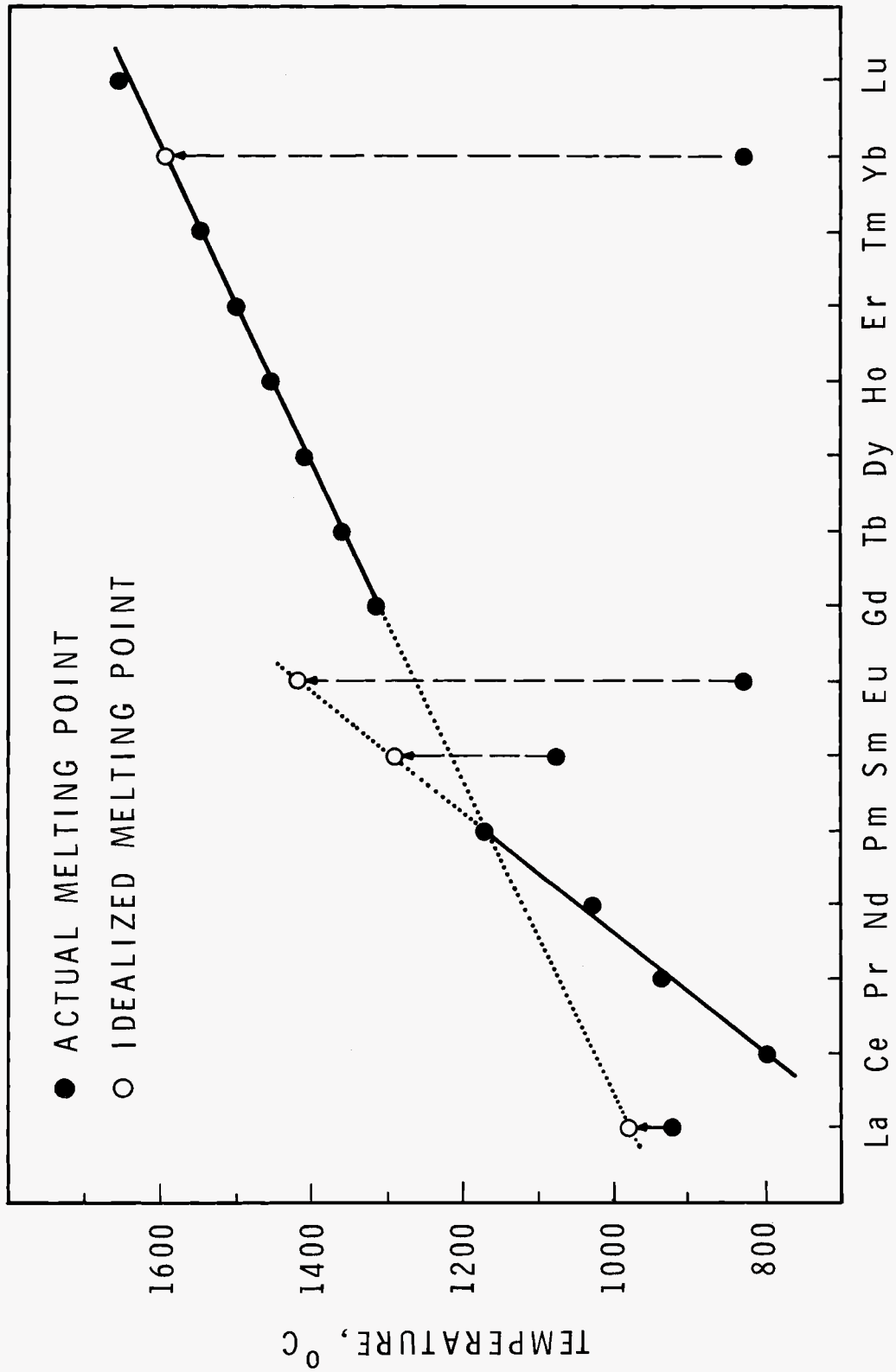

Neg 0684490

FIGURE 4. Melting Points of Rare Earth Metals

7.22 ± 0.02 g/cm^3 measured experimentally. Another exposure was made about two months after the metal was prepared to look at the effect of samarium formation. The extreme darkening of the film by sample radiation makes identification of secondary phases effectively impossible at present. Any change in lattice parameters will therefore be the first indication of the increasing concentration of samarium, and effects of self-radiation damage from the samarium in-growth.

Photomicrographs were taken from an as-cast rod of promethium metal. Metallography is extremely difficult on promethium metal because the self-heat generated increases surface temperatures to the point where oxidation occurs. The technique adopted involved conventional polishing followed by etching with 4% HNO_3 in ethyl alcohol for 1 to 3 sec and examination on the metallograph with a glass slide and immersion oil to minimize oxidation. The microstructure of the as-cast rod is characterized by a fairly large grain size with inclusions (presumably oxide) at the grain boundaries.

MELTING POINT MEASUREMENTS - E. J Wheelwright

The measurement of the promethium metal melting point, 1168 °C, was reported in the previous quarterly[2] and a formal report.[3] The addition of this melting point with those of the other lanthanide metals (Figure 4) suggests some relationships not previously discernible. As with such other properties as the boiling point, heat of vaporization and atomic volume, the melting points of lanthanum, samarium, europium, and ytterbium metal are not "normal," but the behavior can, perhaps, be related to the occupancy of the 4f and 5d energy levels. With both europium and ytterbium, the 5d bonding electron vacates that level and moves into the 4f level. As a result europium and ytterbium melt 590 and 768 °C lower than they would if they retained the "normal" $6S^2 5d^1$

PROMETHIUM METAL PROPERTIES

PREPARATION OF Pm METAL

E. J Wheelwright

The initial phase of this work has been completed. Preparation by calcium reduction of anhydrous $PmCl_3$ has been shown to be feasible, and in excess of 100 g of metal (purity >99%) have been prepared and reported previously.[2,3]

The promethium metal was found to be highly reactive to impurities in the protective argon atmosphere. Work with the other lanthanide metals has shown that the rare-earth metals are much less reactive and are more ductile when the impurity level (particularly oxygen) is reduced to 1 to 10 ppm. Work on development of a method of preparation of ultra-pure promethium metal by the direct reduction of Pm_2O_3 with highly purified lanthanum or thorium metal followed by distillation of the promethium metal, must be postponed until additional funds become available.

PHASE STUDIES

P. G. Pallmer and T. D. Chikalla

The structure of promethium metal at room temperature has been successfully indexed from 14 diffraction lines as double hexagonal. To avoid oxidation, the metal filings were obtained under a fluorinated solvent which provided cooling. The filings will be annealed when a suitably high-purity atmosphere can be provided. The lattice parameters of the hexagonal unit cell were calculated by a best-fit to observed reflections indexed according to the pattern of neodymium. The parameters of the double hexagonal cell were a = 3.68 Å and c = 11.75 Å. The axial ratio of neodymium is 1.614 for c/2a. The values for promethium were comparable, being 1.60 ± 0.01, and 1.62 ± 0.015 a month later. Based on four atoms in the unit cell, the calculated density is 7.31 g/cm^3 which agrees very well with the

The new high temperature thermal diffusivity apparatus was installed in a glove-box during the past month. Debugging and calibration tests will start as soon as installation of the furnace power supply and control system are completed.

all of which were reversible on cooling and quite reproducible. The first occurred at 1915 °C and represents the monoclinic to hexagonal transformation; the second at 2165 °C is probably related to the presence of another high temperature phase recently reported by the French. The melting point was indicated at 2340 °C and agrees very well with the 2350 °C previously reported, as determined by the filament method.

Melting experiments were attempted on Pm_2O_3 in a vacuum of about 10 μ. The photo-diode detection system showed no evidence of melting in the vicinity of 2300 °C and, afterwards, visual examination indicated the 300 mg sample had completely vaporized during the few minutes above 2000 °C, which suggests a quite high vapor pressure for Pm_2O_3. It is noteworthy that in the experiments using Sm_2O_3, under the same conditions, no problems with vaporization occurred.

PROPERTY MEASUREMENTS

R. L. Gibby, R. P. Nelson, and H. T. Blair

Development of the Knudsen cell vapor pressure apparatus has continued. Temperatures as high as 2160 °C have been reached in the crucible while pressures in the 10^{-6} torr range were maintained. Redesign of the r-f feedthrough to eliminate undesired coupling has been found necessary. Calibration of the optical-temperature monitoring system to eliminate absorption effects in the prism and sight window was completed.

Liquid surface tension values are required for an adequate safety analysis of the use of Pm_2O_3 isotopic fuels in earth orbital space missions, and development of a suitable measurement technique has been initiated. Applicability of conventional pendant and sessile-drop techniques is being investigated while a method based on equilibrium meniscus shape as observed by X-radiography is also under consideration.

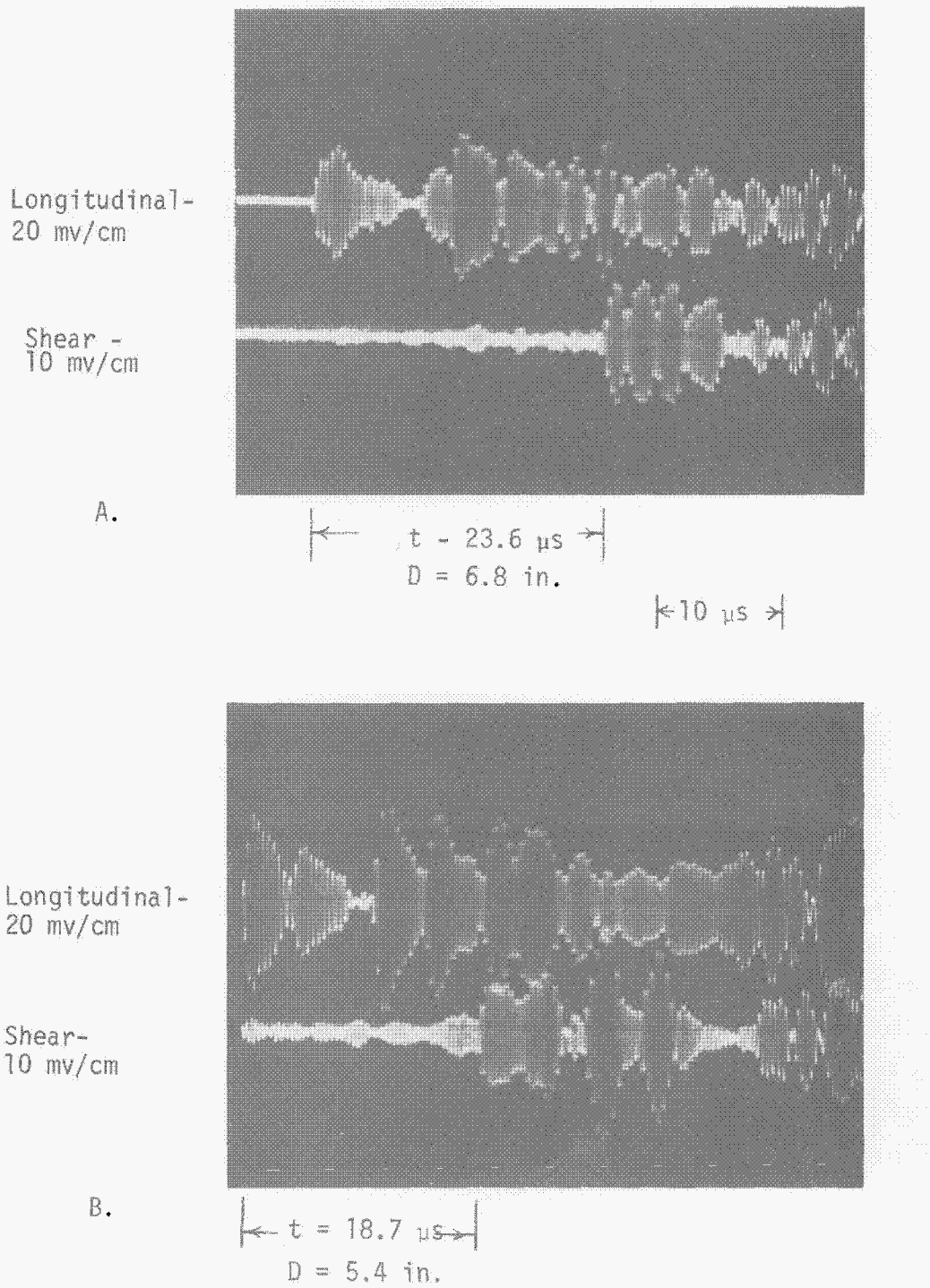

FIGURE 6. Examples of Crack Tip Location Using Longitudinal-Shear Acoustic Emission Components.

near the crack tip to observe the leading edge of both the longitudinal and shear signals. The signal pair shown in Figure 6B, however, was recorded by triggering the oscilloscope directly from the longitudinal signal. This was done to demonstrate the feasibility of using only the longitudinal and shear components of individual acoustic emissions to determine the point of origin of an acoustic emission.

To apply this range-finding technique to the location of flaws along a weld line, signal processing electronics have been developed and demonstrated in breadboard form, which will present the flaw location information on a strip chart recorder. This system will indicate the location of an acoustic-emission source as often as once every second.

Further development of acoustic emission as a nondestructive testing tool requires that a large background of acoustic-emission data be obtained from field tests and correlated with presently used nondestructive techniques.

To obtain this background data, the development of a portable acoustic-emission monitoring system has been initiated. The results of experiments with the laboratory acoustic-emission analysis system were used as guidelines in the development of the portable system. Acoustic-emission signal-processing electronics were designed to convert the emission parameters such as pulse amplitude, average emission power, and emission-source location to a form that can be recorded on a strip chart recorder. In addition, the system includes the capability of presenting the acoustic-emission data to an oscilloscope or magnetic tape recorder. The portable system design incorporates sufficient versatility for application to all types of acoustic-emission monitoring situations, including weld tests, fatigue tests, stress-corrosion cracking experiments, and experiments to determine phase transformation in materials during heat treat.

A feasibility experiment was conducted to identify the problems involved in monitoring acoustic emission from a specimen at high temperature. A weld coupon of 316 SS was cycled repeatedly to 1000 °C while the rate of acoustic emission was monitored. The acoustic-emission source was coupled to the specimen by a strip of 304L SS which extended through the oven wall to allow the sensor to remain outside the oven. (PZT type sensors cannot be operated at temperatures above 320 °C.) For this experiment a surface wave sensor sensitive to frequencies between 0.2 MHz and 0.6 MHz was used. Figure 7 shows the arrangement of the sensor, the acoustic coupler, and the weld coupon. The weld coupon used in this test was a weld in 316 SS that had been contaminated with titanium to produce cracking in the weld. The acoustic coupler was bolted directly to the weld coupon, and surface waves produced by the acoustic emissions were coupled readily from the weld coupon to the acoustic coupler and, hence, to the sensor. Air flow from an electric fan maintained the sensor at a temperature very near room temperature. Acoustic-emission rate as a function of temperature for both the heating and cooling cycles during this experiment is shown in Figure 8. The results of cycling the weld coupon between 500 and 1000 °C repeatedly is shown in Figure 8. No attempt was made to relate the features of this acoustic-emission rate graph to phase transformations in the material since several materials were involved: the 304L coupling rod, the 316 weld coupon, the 308 SS filler metal, and the contaminating titanium in the weld. To verify that the emission signals actually came from the weld coupon and not from the acoustic coupling strip, the weld coupon was removed and the acoustic coupler was cycled from room temperature to 1100 °C. The acoustic emission obtained in this test was less than 10% of the acoustic emission obtained in the one with the weld coupon attached. However, in both tests it was found that the

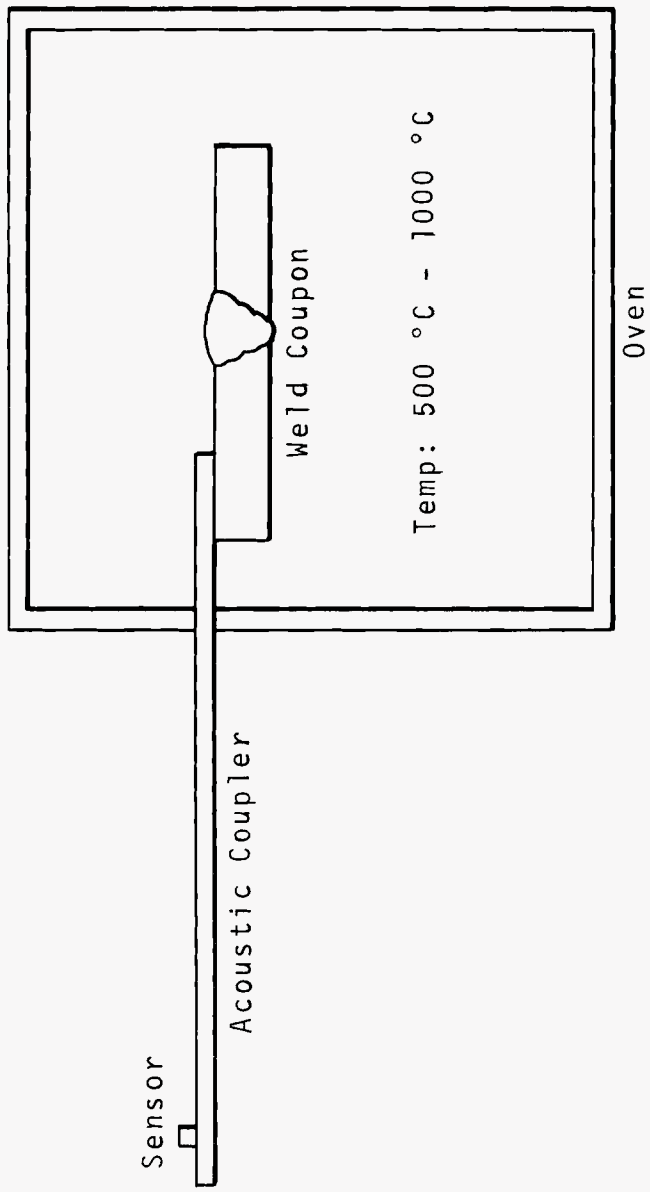

FIGURE 7. *Experimental Arrangement for Receiving Acoustic Emission from a High Temperature Source.*

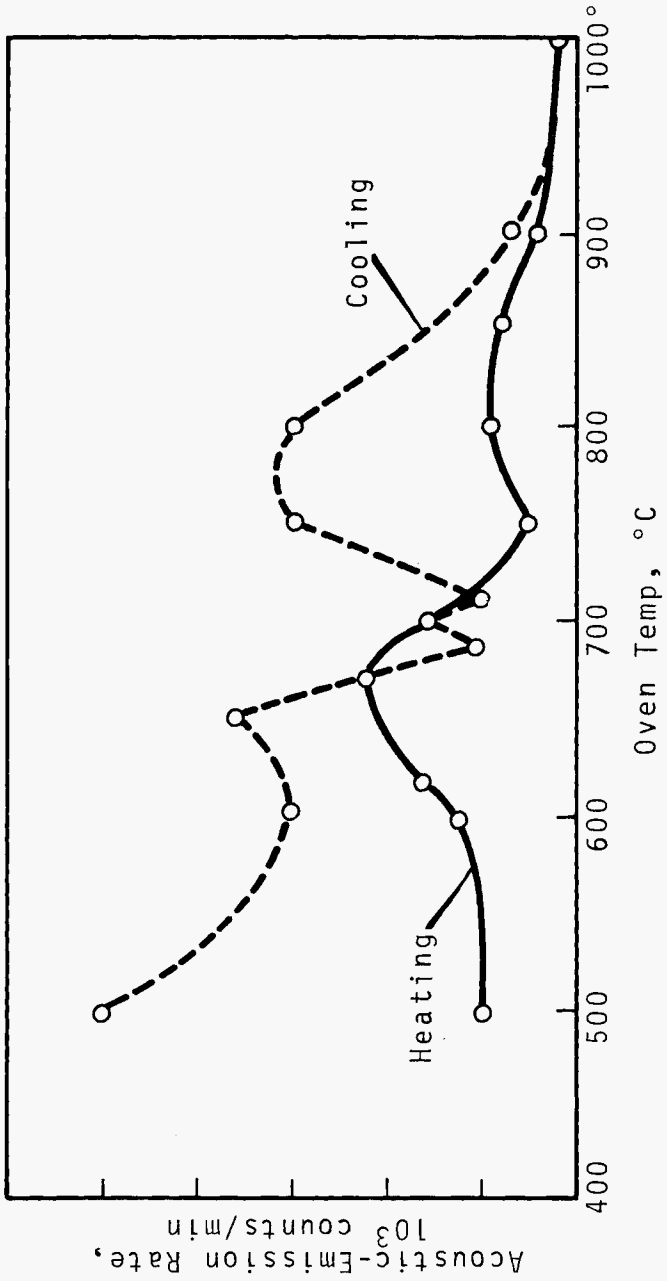

FIGURE 8. *Acoustic Emission Caused by Thermal Cycling a Weld Coupon of 316 SS (weld metal contaminated by titanium).*

acoustic emission dropped to near zero when the temperature approached 1000 °C. In an additional test, a signal was introduced at the sensor by means of an ultrasonic pulsing unit (Figure 9). The graph represents the relative amplitude of the signal reflected from the end of the acoustic coupler in the oven. It shows also that surface wave transmission at the end of the coupler is a strong function of temperature. The signal reflected from the hot (1100 °C) end of the acoustic coupler was reduced to less than 10% of the value obtained at room temperature.

It may be concluded from this test that acoustic-emission data can be readily obtained from material heated to temperatures well above that which an acoustic-emission sensor can tolerate. Type 304L SS is not a good acoustic coupler for temperatures above 600 °C because of the attenuation of the surface wave signal; however, other materials that can stand higher temperatures such as tantalum, molybdenum, fused quartz, or sapphire could be used to extend the high temperature range to well above 1500 °C. Additional experiments of this type will be performed by using the portable acoustic-emission monitoring system now being developed.

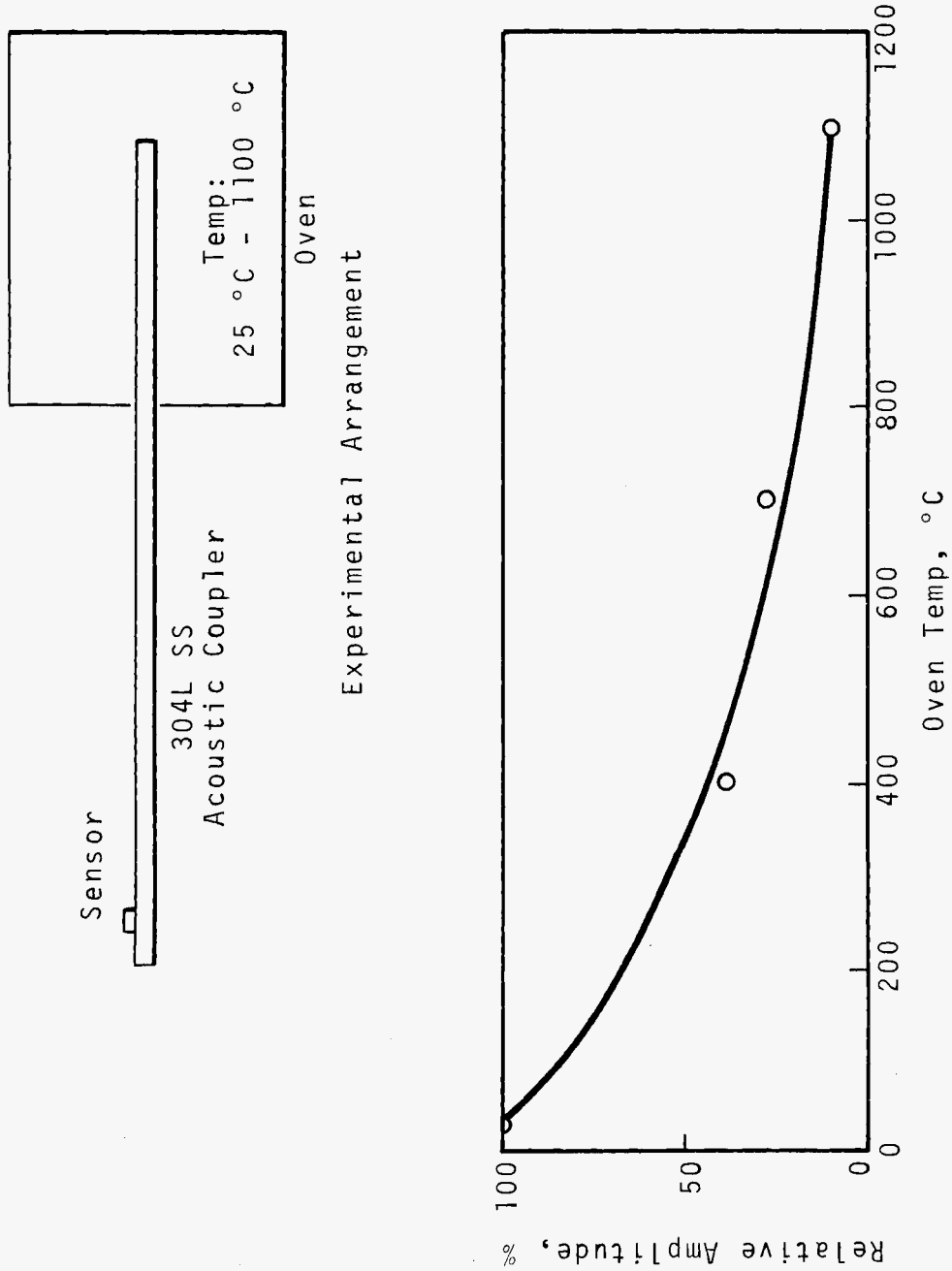

FIGURE 9. Surface Wave Transmission of Acoustic Coupler as a Function of Temperature.

CIRCULATORY SUPPORT SYSTEMS

PROMETHIUM SYSTEMS

F. T. Cross and J. C. Sheppard

The major effort applied to this area was the compilation of the pertinent experimental and theoretical dose-rate data for completing the final report on promethium systems. Presently, the report is in rough draft form.

OTHER RADIOISOTOPES

F. T. Cross and J. C. Sheppard

A review of the literature on fission neutron dosimetry, to better define the problems expected in the ^{238}Pu dosimetry programs, was continued. Some calculations of in-phantom neutron dose-rates for a prototypic 30 W ^{238}Pu source are as follows:

Tissue Thickness, cm	Dose-Rate, rem/hr
2	0.42
4	0.087
6	0.031
8	0.014
10	0.0073

These dose-rate values are the average of three computational sources; the variability being largest in the first few centimeters of tissue.

The complex subsystem designs (heat source and blood pump) of Donald W. Douglas Labs and Aerojet-General have been reduced for computation by the QAD-P5A code, and representative dose-rate values have been calculated.

MODIFICATION OF PROMETHIUM ISOTOPIC COMPOSITION

J. C. Sheppard

Three of the $^{147}Pm_2O_3$ target elements irradiated in a Hanford Reactor were analyzed for their ^{146}Pm content. The final $^{147}Pm_2O_3$ target as well as the Nd_2O_3 target are now being analyzed. These targets, which consisted of two parts (an annular or outer part, and an inner core) had been irradiated to various exposures, and all had been in storage about one year. The period of time allowed most of the 42-day ^{148m}Pm to decay away.

The ^{146}Pm content of these samples was determined in the presence of a large ^{148m}Pm background by the use of an anticoincidence-shielded Ge(li) gamma-ray spectrometer. For these samples the ^{148m}Pm to ^{146}Pm ratio varied between 120 and 1960.

The ^{146}Pm to ^{147}Pm ratios for the three Hanford targets (see table below) indicated that the ^{146}Pm burn-out was the same for the inner and outer target material.

^{146}Pm to ^{147}Pm Ratios for Pm_2O_3 Irradiated in a Hanford Reactor

Target	$^{146}Pm/^{147}Pm$
1	0.16 to 0.19×10^{-6}
2	0.14 to 0.15×10^{-6}
3	0.14×10^{-6}

These results indicate that some ^{146}Pm burn-out has occurred but not as much as expected. Once the results are available for the last Hanford irradiation, cross-sections will be calculated for the appropriate neutrons capture reactions.

Two promethium targets shipped to Savannah River have been irradiated in one of their reactors and will be analyzed in May.

PRODUCTION OF TRANSURANIUM ELEMENTS IN LWR'S

^{241}Am AND ^{238}Pu AVAILABILITY - D. E. Deonigi

A recently published report[1] included availability projections for ^{241}Am recoverable from spent nuclear power fuel reprocessing and projections of ^{238}Pu that could be produced from this ^{241}Am by target irradiation (the report also included projections of a number of other important transuranium and fission product isotopes as well).

The ^{241}Am calculations were based on the quantities of ^{241}Am present in spent fuel at reactor discharge. However, due to the continuing decay of ^{241}Pu (13.2 year half-life), the ^{241}Am content in the spent fuel will continue to increase after reactor discharge up until the time of reprocessing. Reprocessing will not take place for at least three or four months after reactor discharge because of the necessity for a "cooling" period prior to reprocessing. It might conceivably be delayed up to a year, but six-months average delay is more realistic.

The ^{241}Am and ^{238}Pu availabilities have been recalculated (ISOPRO program) by assuming the additional six-months ^{241}Am accumulation from ^{241}Pu decay. The resulting corrected availabilities of ^{241}Am, ^{238}Pu from ^{241}Am, and total ^{238}Pu from all sources (^{237}Np target irradiation, americium target irradiation, and decay of ^{242}Cm recovered directly from spent fuel) are shown in Table 2 for three cases from BNWL-716:[1] Light Water Reactors with no fuel recycle, Light Water Reactors with maximum plutonium recycle, and uranium and plutonium recycle with Fast Breeder Reactor introduction starting in 1980. The quantity of ^{241}Am available is nearly double the quantities reported previously,[1] and the ^{238}Pu from the ^{241}Am is increased a proportional amount. However, the total ^{238}Pu availability is increased only 5 to 10% since the primary

TABLE 2. Annual Availability of ^{241}Am and ^{238}Pu

	Annual ^{241}Am Availability, kg/yr[a]		
	LWRs	LWRs-Pu	LWRs-U/Pu and FBRs
1970	3	3	3
1975	71	71	72
1980	214	349	339
1985	449	1081	879
1990	796	2414	1398
	Annual ^{238}Pu Availability from Americium Target Irradiation, kg/yr		
1970	1	1	1
1975	4	4	4
1980	46	56	54
1985	131	249	241
1990	281	707	547
	Total Annual ^{238}Pu Available from all Sources, kg/yr		
1970	6	6	6
1975	79	79	76
1980	532	527	520
1985	725	808	853
1990	1489	1817	1876

a. *^{241}Am is available only as a mixture of ^{241}Am with ^{243}Am.*

source of ^{238}Pu (^{237}Np target irradiation) is not affected. The ^{238}Pu availability from decay of ^{242}Cm recovered directly from spent fuel is equivalent to about 5 to 10% of the ^{238}Pu from americium irradiation shown in Table 2.

^{250}Cf AND ^{252}Cf AVAILABILITY - D. E. Deonigi

The concentrations of all of the curium, berklium, and californium isotopes involved in the ^{252}Cf production chain have been calculated with the ALTHAEA program for both PWR and BWR equilibrium fuel cycles (Table 3). The cross section data for these calculations are best estimates and involve substantial

TABLE 3. Isotopic Concentrations in Power Reactor Fuels

	PWR		BWR	
	U Enriched	Pu Enriched	U Enriched	Pu Enriched
^{249}Bk, μg/MT	0.338	16.27	0.233	8.50
^{249}Cf, μg/MT	0.055	3.83	0.057	3.02
^{250}Cf, μg/MT	0.075	3.14	0.051	1.55
^{251}Cf, μg/MT	0.019	0.89	0.013	0.43
^{252}Cf, μg/MT	0.006	0.22	0.004	0.094
^{242}Cm, gm/MT	15.07	132.54	14.83	114.58
^{243}Cm, gm/MT	0.13	1.16	0.12	0.95
^{244}Cm, gm/MT	17.34	338.85	14.56	265.00
^{245}Cm, gm/MT	0.84	25.91	0.70	20.17
^{246}Cm, gm/MT	0.102	3.51	0.081	2.46
^{247}Cm, gm/MT	0.0010	0.048	0.0008	0.032
^{248}Cm, gm/MT	0.000046	0.0019	0.000035	0.0011
Exposure	33,000	33,000	27,500	27,500

uncertainties. Because of the successive neutron captures involved in forming these higher isotopes, there is a significant induction period and the composition of lower-exposure startup-cycle fuel would be much lower than the equilibrium cycle compositions in Table 3.

An approximation of ^{250}Cf and ^{252}Cf availability has been prepared by applying the Cf/Cm ratios from Table 3 to the curium availability from BNWL-716 (Table 4). These data should be considered as high-side estimates since there is no adjustment here for the low-exposure startup-cycle effects.

TABLE 4. Annual Availability of ^{250}Cf and ^{252}Cf, μg/yr.

	LWRs	LWRs-Pu	LWRs-U/Pu and FBRs
^{250}Cf			
1970	0.0	0.0	0.0
1975	15.0	15.0	15.0
1980	120.0	260.0	240.0
1985	265.0	1405.0	1320.0
1990	330.0	3610.0	1135.0
^{252}Cf			
1970	0.0	0.0	0.0
1975	1.2	1.2	1.2
1980	9.6	20.8	19.2
1985	21.2	112.4	105.5
1990	26.4	289.0	91.0

REFERENCES

1. *D. E. Deonigi, R. W. McKee, and D. R. Haffner. Isotope Production and Availability from Power Reactors, BNWL-716. Battelle-Northwest, Richland, Washington, July 1968.*

^{237}Np PRICING

As part of a continuing study to develop a rationale for establishing a price for ^{237}Np, ^{238}Pu production costs were developed for a range of cost parameters, and the concentration of ^{236}Pu in ^{238}Pu from power reactor irradiated neptunium targets were investigated.

^{238}Pu COST CALCULATIONS - D. E. Deonigi

The cost of producing ^{238}Pu by target irradiation of ^{237}Np in a PWR (for a range of cost parameters) was calculated with the TAIRCOST program. The range of costs was intended to represent estimated maximum and minimum cost components. The TAIRCOST program calculates a minimum ^{238}Pu production cost at an optimum irradiation time for a given set of cost inputs.

Target irradiation yields were calculated with the ALTHAEA program. The maximum cost of neutrons was based on the additional enrichment required (as calculated by ALTHAEA) to maintain reactivity with the target elements in the reactor. The target elements were assumed to be placed in unused control rod locations. A target density of 1.5 g/cm^3 was used, and the average neutron flux at the targets was determined to be 1.55×10^{13} n/cm^2/sec.

The results of the TAIRCOST calculations are presented here to show the effect of variations in the input costs from a low and high set of base costs. The low and high base cost sets are shown in Table 5, and the ^{238}Pu production costs are tabulated in Table 6 for ^{237}Np values ranging from \$25 to \$100/g.

The ^{238}Pu cost is shown to be highly sensitive to ^{237}Np values, inventory charges, losses and reprocessing charges. The cost appears relatively insensitive to reprocessing time

TABLE 5. Base Cost Sets for ^{238}Pu Production Cost Calculations

	Low Base Costs	High Base Costs
Inventory Charge, %/yr	10	10
Encapsulation and Reprocessing Losses, % each	2	2
Encapsulation Cost, $/kg	400	2,500
Reprocessing Cost, $/kg	2000	15,000
Irradiation Costs		
Handling, $/cm^3	0.1	0.30
Neutrons, $/g	2700	2700
Revenue Loss, $/cm^3-yr	0	3.5
Reprocessing Time, months	4	4

and neutron costs. The variation of ^{238}Pu cost with irradiation time is quite flat (for the PWR irradiation) near the optimum, and a shift of two or four months to coincide with a regular annual refueling would not increase the cost more than 1% for the condition examined here.

^{236}Pu IN ^{238}Pu - D. E. Deonigi

For the investigation of the ^{236}Pu content in ^{238}Pu, an evaluation of the ALTHAEA program's ability to track experimental ^{236}Pu data was first carried out. Table 7 compares the Yankee experimental data[1] with calculated results by use of the ALTHAEA burnup code. It shows good agreement over a wide range of fuel exposures.

The ^{236}Pu content in ^{238}Pu produced by ^{237}Np target irradiation in a PWR were calculated next. The calculation was based on the assumption that target elements would be inserted in unused control rod locations. Although the production of high

TABLE 6. Variation of ^{238}Pu Production Cost with ^{237}Np Target Irradiation Cost Parameters

^{237}Np Value, $/g	Base Cost Set	Cost Component Changed from Base Set	New Value	Optimum Irradiation Time, months	Total Cost of ^{238}Pu, $/g
25	Low	---	---	23.3	110
		Inventory Charge	5%	24.8	91
		Inventory Charge	15%	22.5	129
		Reprocessing Time	8 mo.	25.5	116
		Neutron Cost	$1350/g	24.8	101
	High	---	---	36.0	230
		Inventory Charge	5%	36.0	207
		Inventory Charge	15%	34.5	253
		Reprocessing Time	8 mo.	36.4	234
		Neutron Cost	$1350/g	37.5	219
50	Low	---	---	21.6	186
		Inventory Charge	5%	22.9	148
		Inventory Charge	15%	20.6	223
		Reprocessing Time	8 mo.	23.6	197
		Neutron Cost	$1350/g	22.5	177
		Losses	1%	20.3	177
		Losses	5%	25.1	211
	High	---	---	32.4	310
		Inventory Charge	5%	34.9	268
		Inventory Charge	15%	30.8	352
		Reprocessing Time	8 mo.	33.3	319
		Neutron Cost	$1350/g	33.0	300
		Losses	1%	31.9	302
75	Low	---	---	20.6	261
	High	---	---	29.8	389
100	Low	---	---	20.4	336
		Inventory Charge	5%	21.6	261
		Inventory Charge	15%	19.7	411
		Reprocessing Time	8 mo.	23.3	359
		Neutron Cost	$1350/g	20.6	328
		Losses	5%	24.8	386
	High	---	---	27.6	467
		Inventory Charge	5%	30.8	386
		Inventory Charge	15%	26.3	546
		Reprocessing Time	8 mo.	29.6	486
		Neutron Cost	$1350/g	27.8	458

density NpO_2 target elements was possible, the increased enrichment and flux distortion in the assemblies containing target elements would have been undesirable. Thus, it was assumed that an inert diluent would be added to reduce the target density.

TABLE 7. Comparison of ALTHAEA Calculations with Yankee Experimental Data on $^{236}Pu/^{238}Pu$ Compositions

Yankee Experimental Data[a]			ALTHAEA Calculated Data		
Exposure, MWD/tonne	^{238}Pu nuclei/ barn-cm	$^{236}Pu/^{238}Pu$, ppm	Exposure, MWD/tonne	^{238}Pu nuclei/ barn-cm	$^{236}Pu/^{238}Pu$, ppm
			7,020	0.12×10^{-6}	9.25
8,080	0.14×10^{-6}	9.28			
			10,260	0.29×10^{-6}	9.24
			12,640	0.46×10^{-6}	9.14
13,370	0.47×10^{-6}	9.36			
13,510	0.51×10^{-6}	9.22			
13,630	0.48×10^{-6}	9.17			
			15,210	0.71×10^{-6}	9.01
17,100	0.97×10^{-6}	8.04			
18,860	1.28×10^{-6}	8.12			
			22,660	1.79×10^{-6}	8.49
23,770	2.08×10^{-6}	7.88			

a. *Corrected to reactor discharge date.*

At a target density of 1 g Np/cm^3, the $^{236}Pu/^{238}Pu$ ratio was calculated to be 7 to 8 ppm. By reducing the density to 0.2 g Np/cm^3, the $^{236}Pu/^{238}Pu$ ratio could be reduced to 5 to 6 ppm. A secondary advantage for the lower density is an approximate 30% increase in the target conversion rate. Further density reduction resulted in no more than 10% improvement in ^{236}Pu contamination and did not appear attractive.

If one-half of the fuel assemblies can be used to accept neptunium target rods, all of the neptunium from one reactor could be recycled to the same reactor at a target density of 0.2 g Np/cm^3. This appears a reasonable possibility because only about one-fourth of the fuel assemblies are located to accept a control assembly at any one time.

Further calculations examining the flux shape in a PWR have indicated that the $^{236}Pu/^{238}Pu$ ratio could be reduced to about 1 ppm by placing target elements in the water reflector surrounding the core. This is possible because of the thermal flux peak 1 or 2 in. away from the outer element, and because of the decrease in fast flux (6 MeV) in the reflector. The feasibility and possible additional costs involved in locating target elements in these positions have not been investigated, but any increased cost would have to be balanced off by an increase in ^{238}Pu value with the lower ^{236}Pu content.

REFERENCE

1. *R. C. Smith. Unpublished Data (Private communication), 1968.*

FISSION PRODUCT RHODIUM AND PALLADIUM

RADIATION CHARACTERISTICS OF FISSION PRODUCT Rh and Pd

F. P. Roberts

This new program has the objective to determine the radiation characteristics of rhodium and palladium formed in power reactors. The results of this study will allow an evaluation of the usefulness of these elements as industrial materials and, therefore, assist in deciding whether their recovery deserves serious consideration.

In an earlier investigation* a small quantity of rhodium from 9-yr old Hanford wastes was isolated and purified. This revealed the presence of ^{102m}Rh (2.9 yr half-life) with an abundance of 5 to 10 μCi/g. These findings were more recently substantiated when ARHCO isolated approximately 6 g Rh. This material contained 3.2 μCi ^{102m}Rh/g. Both these samples were from long-cooled wastes (9 yr and 11 yr from reactor discharge). It is believed that short-cooled rhodium will also contain ^{102}Rh (200 days half-life) as well as lesser amounts of ^{101}Rh (3.1 yr half-life). All these isotopes are gamma emitters and, if present in large quantities, could give rise to serious dose rates.

Fission product palladium contains 20% ^{107}Pd which decays by emission of a 0.035 MeV beta with a half-life of 7×10^6 yr. Because of the low energy of decay and the long half-life, it is believed that problems caused by radioactivity will not restrict its use. However, this must be verified.

A 10 kg sample of irradiated, Yankee Reactor fuel is on site and available to this program. Dissolution of this fuel has been started, and potential rhodium and palladium separation methods are being tested in the laboratory.

---

* *Funded by the Division of Production.*

DISTRIBUTION

No. of Copies	
OFFSITE	
2	AEC Albuquerque Operations Office
1	AEC Chicago Patent Group G. H. Lee
197	AEC Division of Technical Information Extension
20	AEC Library, Washington J. N. Maddox (DID) (4) W. K. Eister (DID) E. E. Fowler (DID) G. Y. Jordy (DID) G. A. Newby (SNS) R. T. Carpenter (SNS) F. C. Schwenk (SNS) G. P. Dix (SNS) J. A. Powers (SNS) J. S. Griffo (SNS) W. K. Kern (SNS) M. Klein (SNS) M. Shaw (DRDT) S. Seiken (DRDT) F. P. Baranowski (DP) G. B. Pleat (DP) W. Lenneman (DP)
1	AEC New York Operations Office
2	AEC Oak Ridge Operations Office J. H. Kahn Dent C. Davis
1	AEC Sandia Area Office
1	AEC Savannah River Operations Office
2	Aerojet-General Corporation (NASA)
1	Aerojet-General Nucleonics (SAN) W. G. Ruehl
1	Aerojet-General Corporation, San Ramon (NASA)

No. of Copies	
1	Aerospace Corporation, Los Angeles (AF)
1	Airesearch Manufacturing Company, Los Angeles
2	Air Force Aeronautical Systems Division
1	Air Force Air University Library
1	Air Force Headquarters
2	Air Force Weapons Laboratory
1	Army Reactors Field Group
1	Aro, Inc. (AF)
2	Avco Corporation (NASA) R. Y. Parkinson (1)
1	Bellcomm, Incorporated (NASA)
1	Bendix Corporation (NASA)
1	Central Intelligence Agency
2	Douglas Aircraft Corporation, MSSD (AF)
2	du Pont Company, Aiken (AEC) D. H. Turno W. D. Sandberg
1	General Electric Company (AEC) (NASA)
2	General Electric Company (MSD) (AEC)
1	General Electric Company, MSVD; Cincinnati M. Bromberg
1	General Electric Company, MSVD; Valley Forge P. E. Brown
1	General Electric Company, Vallicitos Laboratory L. P. Bupp
1	Grumman Aircraft Engineering Corporation (NASA)
1	Hittman Associates, Inc. (AEC)
2	Hughes Aircraft Company, Aerospace Group, Culver City, California F. N. Magee K. W. Cowans

No. of Copies	
1	Hughes Aircraft Company, Malibu (AF)
1	Institute for Defense Analyses (ARPA)
1	Isotopes Inc., Middle River (AEC)
1	Lockheed-Georgia Company (NASA)
1	Massachusetts Institute of Technology (AEC)
1	Massachusetts Institute of Technology (Lincoln) (AF)
2	Mound Laboratory (AEC)
	G. R. Grove
	R. L. Neubert
1	NASA Ames Research Center
4	NASA Goddard Space Flight Center
	W. C. Isley (1)
1	NASA Langley Research Center
1	NASA Lewis Research Center
	Lloyd Shure
2	NASA Manned Spacecraft Center
	Anthony Redding (1)
4	NASA Marshall Space Flight Center
2	NASA, Washington
4	National Reactor Testing Station (Inc) (AEC)
1	Navy, Nuclear Power Division (Washington)
	Graham Haigie (NAVFAC)
1	Navy Air Development Center
1	Navy Air Systems Command
1	Navy Facilities Engineering Command
1	Navy Office of the Chief of Naval Operations
3	Navy Ordnance Systems Command
1	Navy Radiological Defense Laboratory
	F. Kawahara

No. of Copies	
1	Navy Space Systems Activity
1	Nuclear Materials and Equipment Corporation (AEC)
	C. S. Caldwell
4	Oak Ridge National Laboratory (AEC)
	P. S. Baker
	A. F. Rupp
	E. Lamb
	S. J. Rimshaw
1	Public Health Service (HEW)
1	Radio Corporation of America (AEC)
1	Radio Corporation of America, Cranbury (AEC)
1	Rand Corporation (AF)
1	Republic Aviation Division (NASA)
1	Sanders Nuclear Corp., Nashua, N. H.
	Douglas Harvey
2	Sandia Corporation, Albuquerque (AEC)
	V. E. Blake
	A. J. Clark
1	Tracerlab, Richmond (AF)
1	TRW Space Technology Labs, Redondo Beach, Calif.
	W. M. Bowes
1	TRW Systems (AEC)
1	Westinghouse Electric Corporation, Lima (NASA)
1	Wright-Patterson AFB, Dayton, Ohio
	Capt. D. C. De Pree

ONSITE-HANFORD

1	AEC Chicago Patent Group
	R. K. Sharp (Richland)

No. of Copies	
2	AEC RDT Site Representative
	P. G. Holsted
2	AEC Richland Operations Office
	C. L. Robinson
	B. A. Ryan
7	Atlantic Richfield Hanford Company
	S. J. Beard
	J. S. Cochran
	H. H. Hopkins
	H. C. Rathvon
	P. W. Smith
	R. E. Tomlinson
	M. J. Szulinski
3	Battelle Memorial Institute
3	Donald W. Douglas Laboratories
	R. L. Andelin
	R. S. Cooper
	Files
5	Douglas United Nuclear
	T. W. Ambrose
	R. G. Geier
	M. Lewis
	R. Nilson
	W. K. Woods
50	Battelle-Northwest
	J. M. Atwood
	E. A. Berreth/C. G. McCormack
	A. G. Blasewitz
	D. W. Brite
	R. E. Burns
	J. J. Cadwell
	T. D. Chikalla
	C. R. Cooley
	F. T. Cross
	G. M. Dalen
	R. L. Dillon
	D. R. de Halas
	C. J. Denton

Battelle-Northwest (contd)

D. E. Deonigi
K. Drumheller
E. A. Evans
P. L. Farnsworth
J. C. Fox
H. T. Fullam
V. L. Hammond
H. Harty
A. J. Haverfield
J. A. Jarrett
J. N. Judy
H. A. Kornberg/R. C. Thompson
C. E. Leach
R. W. McKee/E. T. Merrill
R. L. Moore
C. E. Newton, Jr.
R. E. Nightingale
H. M. Parker
R. S. Paul
A. M. Platt
F. P. Roberts
R. K. Robinson
C. A. Rohrmann
W. W. Schulz
R. J. Sorenson
J. C. Spanner
H. H. Van Tuyl
C. E. Vogel
E. E. Voiland
E. J Wheelwright
Technical Information Files (5)
Technical Publications (2)